Control of Heme Reactivity by Diffusion: Structural Basis and Functional Characterization in Hemoglobin Mutants[†,‡]

Adriana Erica Miele,[§] Federica Draghi, Alessandro Arcovito, Andrea Bellelli, Maurizio Brunori,* Carlo Travaglini-Allocatelli, and Beatrice Vallone

Department of Biochemical Sciences "A. Rossi Fanelli" and CNR Centre for Molecular Biology, University of Rome "La Sapienza", P.le A. Moro 5, 00185 Rome, Italy

Received August 2, 2001; Revised Manuscript Received September 24, 2001

ABSTRACT: The effect of mutagenesis on O_2, CO, and NO binding to mutants of human hemoglobin, designed to modify some features of the reactivity that hinder use of hemoglobin solutions as blood substitute, has been extensively investigated. The kinetics may be interpreted in the framework of the Monod-Wyman-Changeux two-state allosteric model, based on the high-resolution crystallographic structures of the mutants and taking into account the control of heme reactivity by the distal side mutations. The mutations involve residues at topological position B10 and E7, i.e., Leu (B10) to Tyr and His (E7) to Gln, on either the α chains alone (yielding the hybrid tetramer Hbα^{YQ}), the β chains alone (hybrid tetramer Hbβ^{YQ}), or both types of chains (Hb^{YQ}). Our data indicate that the two mutations affect ligand diffusion into the pocket, leading to proteins with low affinity for O_2 and CO, and especially with reduced reactivity toward NO, a difficult goal to achieve. The observed kinetic heterogeneity between the α^{YQ} and β^{YQ} chains in Hb^{YQ} has been rationalized on the basis of the three-dimensional structure of the active site. Furthermore, we report for the first time an experiment of partial CO binding, selective for the β chains, to high salt crystals of the mutant Hb^{YQ} in the T-state; these crystallographic data may be interpreted as "snapshots" of the initial events possibly occurring on ligand binding to the T-allosteric state of this peculiar mutant Hb.

Hemoglobins are widely distributed among animal phyla, ranging from arthropoda and anellida to vertebrata; moreover, they have been described in bacteria (*1*). Although the primary function of the protein in mammals is oxygen and carbon dioxide transport, it is known that it also exhibits oxido-reductase activity toward several substrates, most notably NO. The variety of physiological functions attributed to Hb and the extreme differences in O_2 availability characteristic of the environments colonized by Hb-carrying animals require fine modulation of reactivity, which is accomplished by changes in the protein moiety, given that the heme group is invariant (*2*).

Clarification of structure−function relationships of different Hbs is demanding, since it requires determination of the functional properties and the high resolution 3D structures of different derivatives of the wild-type Hb of choice and its most relevant site-directed mutants. So far, a protein-engineering approach has been applied mostly to human HbA because of its possible medical relevance and biotechnological applications, notably because large-scale bacterial expression biosynthesis of mutated HbA may lead to products suitable for intravenous administration (*3*, *4*). These preparations, usually referred to as blood substitutes, may induce several adverse reactions, due either to contaminant toxins or lipidic remnants of the red cell membrane or to intrinsic properties of Hb which once extracted from the red blood cell, is characterized by a physiologically elevated oxygen affinity (*2*). Moreover, the high reactivity versus NO leads to sequestration of this messanger and thereby intense vasoconstriction and local hypoxia (*5*). Therefore, an important objective for site-directed mutagenesis of HbA is that of reducing its reactivity toward NO.

The reactivity of Hb toward its ligands is mainly regulated by the proximal His(F8), which pulls the iron out of the heme plane (*6*), and by amino acid residues on the distal side of the heme, i.e., the ligand pocket. The latter offer much richer opportunities to finely modulate the control of ligand affinity and the discrimination between different ligands (*7*, *8*). Dioxygen, the physiological ligand of Hb, has a relatively low affinity for the heme iron, but is easily stabilized by H-bonding to a distal residue, i.e. His (in almost all vertebrate Hbs and Mbs and in many invertebrate Hbs) or Gln at position E7 (*9*). When the distal His is mutated to a non-H-bonding residue, the O_2 affinity of Mb and the α chains of Hb is dramatically lowered, while the β chains are scarcely affected (*7*, *10*). Since the same substitutions have a much smaller and less predictable effect on CO binding, the CO/O_2 partition constant of His (E7) mutants of Hbs and Mbs is usually much increased.

[†] This work was supported by the CNR Project "Biotechnology" (legge 95/95).

[‡] Coordinates of deoxy Hbα^{YQ}, deoxy Hbβ^{YQ}, and Hb^{YQ}-CO have been deposited in the Protein Data Bank (accession numbers 1J7S, 1J7W, and 1J7Y, respectively).

* To whom correspondence should be addressed. Phone: +39-06-4450291. Fax: +39-06-4440062. E-mail: maurizio.brunori@uniroma.it.

[§] Research fellow of the Istituto Pasteur-Fondazione Cenci Bolognetti.

10.1021/bi011602d CCC: $20.00
Published on Web 11/07/2001

The control of Hb reactivity toward NO proved more difficult. This gas has an extremely high affinity for Hb and Mb, its reaction being diffusion limited (*11, 12*). Moreover, NO is unique in its ability to react with deoxy, oxy, and ferric Hb:

$$Hb + NO \rightarrow HbNO \quad (1)$$

$$HbO_2 + NO \rightarrow Hb^+ + NO_3^- \quad (2)$$

$$Hb^+ + NO \rightarrow Hb^+NO \rightarrow Hb + NO^+ \quad (3)$$

Reaction 1 yields the high-affinity NO complex, whose dissociation half time is extremely long (*13*). Reaction 2 is probably prevailing in vivo because of the dominance of HbO_2 even in venous blood; it is further favored if a preparation based on free, extracellular Hb is injected intravenously. Reaction 3 yields a low-affinity complex and is scarcely relevant in vivo.

Since the reactivity of the ferrous heme iron versus NO is so high, a possible strategy to achieve its reduction involves an increase in the external diffusive barrier to ligand binding (*11*, *12*, *14*), which may be obtained by mutating residues on the distal side, most notably His(E7), which gates the access to the heme (*15*). Alternative to His at position E7 is Gln, which is known to make a H-bond with bound O_2 and is present in some invertebrate Hbs, in elephant Mb and in the α chains of opossum Hb (*16*−*18*). A residue frequently coupled to Gln(E7) in invertebrate Hbs is Tyr(B10); the couple Gln(E7) and Tyr (B10) may thus be expected to have special functional relevance.

Previous work (*19*−*21*) showed that the two mutations His(E7) → Gln and Leu (B10) → Tyr exert the following effects when inserted in the sequence of sperm whale Mb: (i) the O_2 affinity is maintained or slightly decreased; (ii) the rate constants for O_2 combination and dissociation are both decreased, and (iii) the autoxidation rate is lowered. Basically, the decreased rate constant for O_2 combination may be ascribed to the crowding of the heme pocket, whereas the decreased rate constant for O_2 dissociation is attributed to an additional H-bond donated by Tyr(B10) (*20*, *21*). Recently, these two mutations were inserted in both chains of HbA and were demonstrated to slow significantly the combination rate constants of all ligands tested (*22*), as expected on the basis of the hypothesis that they inhibit the diffusion of the ligand toward the heme iron.

This paper reports an extensive characterization of the reactions with O_2, CO, and NO of human HbA bearing the double mutation Leu(B10) → Tyr and His(E7) → Gln on the α, the *β*, or both chains (the corresponding Hb tetramers being called $Hb\alpha^{YQ}$, $Hb\beta^{YQ}$, and Hb^{YQ}, respectively). Moreover, the structure of the deoxygenated derivative of the three mutant hemoglobins, determined at high resolution from crystals grown in high salt concentration, sheds light on the present and the previously reported functional information. Finally, we determined the structure of partially CO-saturated Hb^{YQ} and demonstrated that the ligand combines almost exclusively with the heme of the *β* chains.

In Hb, the structural basis of the control of ligand reactivity is much more complex than in Mb since it arises from the interplay of two allosteric states (called T and R) and two types of chains. The structural information and the extensive kinetic investigation herein reported allow the interpretation of the behavior of the three YQ mutants of HbA yielding a consistent picture and providing information which may prove useful for the rational design of mutated Hbs suitable for use as blood substitutes.

Table 1: Summary of Crystal Parameters for the Structures of the Deoxygenated YQ Mutants

	$Hb\alpha^{YQ}$	$Hb\beta^{YQ}$	$^{T}Hb^{YQ}CO$
resolution range (Å)	18.0−2.2	30.0−2.0	30.0−1.7
R_{merge} (%)	5.4	8.5	4.3
mosaicity	0.6	0.98	0.51
completeness (last shell) (%)	96.3 (94.2)	94.2 (93.8)	99.8 (98.5)
multiplicity	4.6	3.2	6.5
space group	$P2_1$	$P2_1$	$P2_1$
cell parameters			
a (Å)	63.2	63.4	62.9
b (Å)	84.0	84.3	84.1
c (Å)	53.9	53.8	54.1
d (deg)	99.2	99.4	99.3
R_{cryst} (R_{free}) (%)	19.4 (22.5)	17.1 (22.3)	15.5 (20.1)

EXPERIMENTAL PROCEDURES

The recombinant mutant hemoglobins were expressed in *Escherichia coli* and purified to homogeneity as previously reported (*22*, *23*). All experiments were carried out in 0.1 M bisTris/HCl, pH 7.0, at 20 °C, unless otherwise specified; reagents were of analytical grade.

The time courses of ligand binding or release have been measured using an Applied Photophysics MV17 stopped flow apparatus (Leatherhead, U.K.). Geminate rebinding kinetics have been followed in a pulsed CCD camera after laser photolysis with a Nd:YAG pulsed laser at 532 nm and power 100 mJ pulse. Protein concentration ranged from 2 to 10 μM heme. At these Hb concentrations, dissociation into dimers occurs only in the presence of heme ligands (CO, O_2 or NO); since dimers behave like R state Hb, they do not influence partial photolysis experiments or ligand replacements (*2*). Basically, there is one type of experiment whose result is influenced by the presence of dimers, i.e., the time course of O_2 dissociation by dithionite, which may present a slow dissociating component, not included in the data analysis.

Crystals of the deoxygenated derivatives of $Hb\alpha^{YQ}$, $Hb\beta^{YQ}$, and Hb^{YQ} were grown after batch crystallization in high-salt conditions (*24*) in an anaerobic chamber (Belle Technology, U.K.). Partially liganded crystals of $^{T}Hb^{YQ}$ were obtained after soaking the deoxygenated crystals with mother liquor equilibrated with 1 mM CO, in the presence of sodium dithionite in order to avoid iron oxidation. X-ray data were collected using a Rigaku R-axisII image plate ($Hb\alpha^{YQ}$, $Hb\beta^{YQ}$) or a R-AxisIV^{2+} image plate (Hb^{YQ}-CO bound) system and a rotating anode X-ray generator. The deoxygenated derivatives were collected at room temperature on capillary-mounted crystals. The partially liganded mutant was collected at 100 K, using 25% glycerol as cryoprotectant.

A summary of data collection statistics is given in Table 1. Data were indexed and scaled using HKL package (*25*) and refined to the final resolution using the program Refmac (*26*) of the CCP4 suite (*27*). The starting model for refinement of both the deoxygenated structures was human deoxy Hb collected at room temperature [PDB code 2HHB (*28*)], from which the solvent molecules had been removed and side chains of the mutated residues converted into Gly.

For the refinement of $^{T}Hb^{YQ}$-CO, the deoxygenated structure of the same mutant has been used [PDB code 1QI8 (*22*)]. Water molecules were added using the X-solvate program (Quanta, MSI Inc.) but they were kept only if consistently positioned and their *B*-factor was lower than 40. Inspection of the final protein structures was performed with Procheck (*29*), which showed satisfactory statistics, consistently with the resolution of the starting data.

RESULTS

The reactivity of the Hb mutants (hereafter called YQ) was studied on the double mutant (i.e., the tetramer Hb^{YQ} in which both chains are mutated) and on the hybrid tetramers bearing the two mutations on either the α or the *β* chain only (called $Hb\alpha^{YQ}$ or $Hb\beta^{YQ}$, respectively). O_2 dissociation curves of the double and hybrid mutants (*22*) showed that despite the reduced affinity, they are both cooperative. Upon saturation with O_2 or CO, all the mutants undergo a quaternary transition from the T to the R-state, as indicated by markers of the allosteric state, such as the optical spectrum of the heme (especially in the Soret region) and the perturbation of the Trp*β*(37)at the $\alpha_1\beta_2$ subunit interface (*30*, *31*). Moreover, it has been shown (A.E.M. and F.D., unpublished data) that the Bohr effect of Hb^{YQ} is normal. Since the direct effect of the mutated side chains in the distal pocket on the intrinsic reactivity of the heme cannot be easily distinguished from possible perturbations of the quaternary conformational change, a quantitative description of the allosteric properties of these Hbs from equilibrium data is difficult. Therefore, we have carried out a number of diagnostic kinetic experiments in order to explore separately the functional properties of the two allosteric states and, thus, test the possibility of describing the data within the framework of the MWC model (*32*, *33*). As a necessary prerequisite, we have solved the three-dimensional structure of the mutants in the deoxygenated or partially liganded form, to propose a structural interpretation of the functional data.

Structural Properties. (i) Deoxygenated Mutant Hbs. Highly diffracting crystals of the deoxygenated derivatives of the two hybrid proteins have been obtained under Perutz's high salt conditions (see Experimental Procedures). The structures resulted from the merging of room-temperature data collected on two single crystals. Crystals of $Hb\alpha^{YQ}$, though diffracting only to 2.2 Å, were well ordered with a mosaicity of 0.6; on the other hand $Hb\beta^{YQ}$ diffracted well up to 2.0 Å, but were much less ordered, as can be judged by a mosaicity value of 0.98. Nonetheless, the packing in both protein crystals was very tight (around 63% of the cell being occupied by protein atoms), with one tetramer per asymmetric unit. None of the amino acids of the final structure lies in forbidden zones of the Ramachandran plot. Statistics on the geometry is very good for both crystals, with rms deviations from ideal bond length and angles negligible; only 23 and 18 residues in $Hb\alpha^{YQ}$ and $Hb\beta^{YQ}$, respectively, of 854 residues had standard deviation values of >2.

The overall quaternary structure and the tertiary fold of the three mutants are completely unchanged compared to wild-type (wt) deoxy HbA (*28*, *34*); in particular, the subunit interfaces are unperturbed, showing that all mutants are in the T allosteric state. Differences with respect to wt deoxy HbA are limited to the residues of the distal heme-binding pocket bearing the mutations and to related solvent molecules (Figure 1). In both hybrid proteins, the wt chain is unchanged with respect to HbA; furthermore, in each of the two hybrids $Hb\alpha^{YQ}$ and $Hb\beta^{YQ}$, the structure of the mutated pocket is superimposable on that of deoxy Hb^{YQ}, even in terms of distances between residues. The distal side of the heme pocket of the mutated α chains of Hb^{YQ} is somewhat smaller and more crowded than that of the mutated *β* chains; this condition is the opposite of the one occurring in wt HbA (*35*). Moreover, in all the mutants there is a network of hydrogen bonds, which keeps the mutated residues, Tyr and Gln, firmly connected to the heme propionates via a water molecule. Remarkably, in one of the two wild-type α chainsof $Hb\beta^{YQ}$, there is electron density for one water molecule, as shown for HbA (*28*). Thus, the crystallographic data show that the mutations in one chain do not affect the tertiary folding of the partner wt chain in each hybrid mutant.

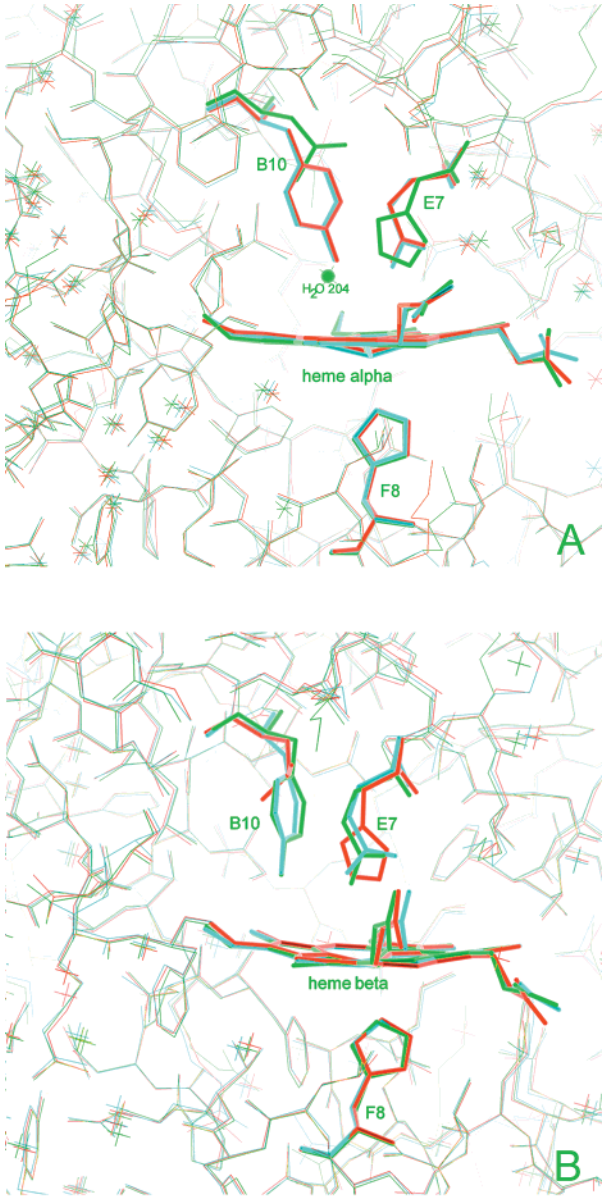

FIGURE 1: Superposition of the deoxygenated structures of $Hb\alpha^{YQ}$ (red), $Hb\beta^{YQ}$ (green), and Hb^{YQ} (blue). Panel A depicts α chains and panel B *β* chains. Residues B10, E7, F8, and the heme are presented in stick; the water molecule found in the pocket of wt α chain of $Hb\beta^{YQ}$ is drawn as a ball.

In conclusion, in the T allosteric state, the structural features of Tyr (B10) and Gln(E7) in the distal pocket of the α or β chains of the hybrid Hbs as well as in Hb^{YQ} are identical.

This structural information suggests a simple interpretation for the kinetic results reported below, based on the hypothesis that in all the YQ mutants ligand binding should be easier (and possibly faster) in the β^{YQ} chains because of a wider distal pocket and a weaker H-bonding network, in the T-state molecule.

(ii) $^{T}Hb^{YQ}$-CO. The peculiar properties of the mutant Hb^{YQ}, namely the low ligand affinity and possibly the high switch-over point (*22*), made it possible to study the structure of a partially liganded T-state hemoglobin. We have collected data from four different CO-soaked Hb^{YQ} crystals and observed consistently that CO is bound to the β chains only, while the molecule remains in the T-quaternary state, as judged from inspection of the $\alpha_1\beta_2$ interface. This observation is the first and most obvious experimental result consistent with the hypothesis outlined above, i.e. that accessibility of the β^{YQ} chain is greater than that of the α^{YQ} chain. We present the structural features of $^{T}Hb^{YQ}$ with CO bound to both β chains and compare this structure with that of the same molecule in the deoxy state [1QI8 (*22*)], with deoxy HbA [2HHB (*28*)], and with $^{T}HbA\text{-}O_2$ grown in low salt condition (*36*).

Soaking with CO does not affect the quality of the crystals, which start cracking and dissolving only after 24 h soaking. The final model of $^{T}Hb^{YQ}$-CO comprises 854 residues, 4 heme groups, 2 CO molecules, 2 sulfate groups, and 441 water molecules. The overall crystallographic *R*-factor converged to a value of 15.5% for data ranging from 30.0 to 1.7 Å. The stereochemistry of bond angles and bond length is very good with rms of 1.64° and 0.01 Å, with respect to ideal bond angle and length. The mean *B*-factor calculated with *B* average (*27*) on the complete structure (solvent included) is 21.85 $Å^2$. The tertiary and quaternary structure is almost the same as deoxy HbA and deoxy Hb^{YQ}, with overall rms displacement of all the atoms of, respectively, 0.42 and 0.32 Å. Differences are almost totally localized in the heme pocket of the β chains, but minor adjustments of main and side chains can be envisaged also in the unliganded α chains and at the $\alpha_1\beta_2$ interface.

The most important result is the clear appearance on both β chains of electron density for a diatomic molecule, consistent with a bound CO. The occupancy has been satisfactorily refined in both cases to unity, since no positive or negative peaks in the $F_o - F_c$ associated difference map appeared. The *B* temperature factors associated with the iron and the CO atoms are consistent with a bound conformation. In Table 2, distances between the mutated side chains and with the heme in the four subunits of Hb^{YQ} and $^{T}Hb^{YQ}$-CO are reported. As stated above, the general architecture of the distal side of the heme pocket, i.e. the overall position of helices B and E, is not the same for α and β chains, the former being more tightened-up and compact. Crowding of the heme pocket prevents ligands from binding without a substantial displacement of the side chains and breaking of the H-bond network present in the deoxy state. On the other hand, looking at the values in bold reported in Table 2, the β chains face a more "open" pocket, wide enough to let a diatomic ligand approach the iron for binding.

Table 2: Distances (Å) between the Mutated Amino Acids and the Heme Environment for Unliganded and Partially Liganded Hb^{YQ}

	Hb^{YQ}				$^{T}Hb^{YQ}$-CO			
from → to	α_1	α_2	β_1	β_2	α_1	α_2	β_1	β_2
Tyr (OH) → Gln(NH_2)	3.2	3.3	3.3	3.4	3.2	3.2	5.1 5.3	3.5
Gln(C=O) → H_2O	2.7	2.7	3.5	2.6	2.6	2.6	3.0	2.5
H_{2O} → heme (propionate)	2.8	2.7	2.5	2.7	2.8	2.7	2.7	2.5
Tyr (OH) → Fe	**4.0**	**4.2**	**4.8**	**5.1**	3.8	3.9	4.4	4.9
Gln(NH_2) → Fe	3.9	4.0	4.4	4.3	3.8	3.8	5.0	4.4
Tyr (OH) → CO (O)							2.5 5.3	3.6
Gln(NH_2) → CO (O)							3.4	2.5

Experiments of ligand binding to crystals and extensive binding studies on normal, mutant, and iron-substituted Hbs available in the literature (*37*−*40*) convey the picture that in HbA the α chains have a ligand affinity higher than the β chains and, furthermore, that the effects of distal mutations are smaller for the β chains. In the case of Hb^{YQ}, the peculiar and asymmetric structural organization of the mutated side chains seems to account for the enhanced reactivity of the β^{YQ} compared to the α^{YQ} chains (see also below). An unexpected feature observed in the doubly liganded $^{T}Hb^{YQ}$-CO is an asymmetry between the two liganded β^{YQ} chains, which we believe to be due to crystal packing. The $\beta_2{}^{YQ}$ chain is in close contact with residues of the $\alpha_2{}^{YQ}$ chain of another symmetry-related tetramer, while $\beta_1{}^{YQ}$ is facing the solvent. This is reflected in the position of the mutated side chains. In $\beta_2{}^{YQ}$, motion of the side chains of Tyr (B10), Gln-(E7), Phe (CD2), and Val (E10) is relatively small with respect to deoxy Hb^{YQ} (see Figure 2B compared to deoxy α^{YQ} chain shown in Figure 2A). Binding of CO is associated with a motion of the iron atom into the heme plane, which still remains tilted, and a shift of the proximal His (F8), the Fe−His bond length remaining at 2.2 Å. Tyr (B10) and Gln (E7) move slightly toward the outside, as can be seen from Table 2. It is not unreasonable that this structure represents a bound T-state. In fact, due to crystal-packing contacts, tertiary changes are limited to the minimal motions necessary to allow ligand coordination. Thus, it may be taken as a "snapshot" of the very first events of ligand binding to a t-state subunit in a T-state molecule (*41*). Of course, extrapolation of this observation to wt HbA may be hazardous, given that in HbA the heme pocket is more closely packed in the β rather than in the α chains (*28*, *42*).

On the other hand, in $\beta_1{}^{YQ}$ we face a different set of events (Figure 2, panels C and D). The absence of packing constraints allows more mobility to the side chains, which move upon CO binding; the bound ligand experiences a different orientation compared to $\beta_2{}^{YQ}$. Noteworthy in $\beta_2{}^{YQ}$, Tyr(B10) is present in two alternative conformations, which have been refined with 50% occupancy for each conformer, with no residual positive or negative difference electron density in the final model; these are shown in Figure 2, panels C and D. Furthermore, the amide group of Gln(E7) rotates toward the solvent (best seen in Figure 2D), establishing only a loose contact with the oxygen atom of CO (3.4 Å). The H-bond network between Gln(E7), water no. 125, and the heme propionate is preserved, but we observe a concerted motion coupled to CO binding. The diatomic ligand is positioned in a more canonical way, even with respect to the bond angle; the heme displays a more planar configu-

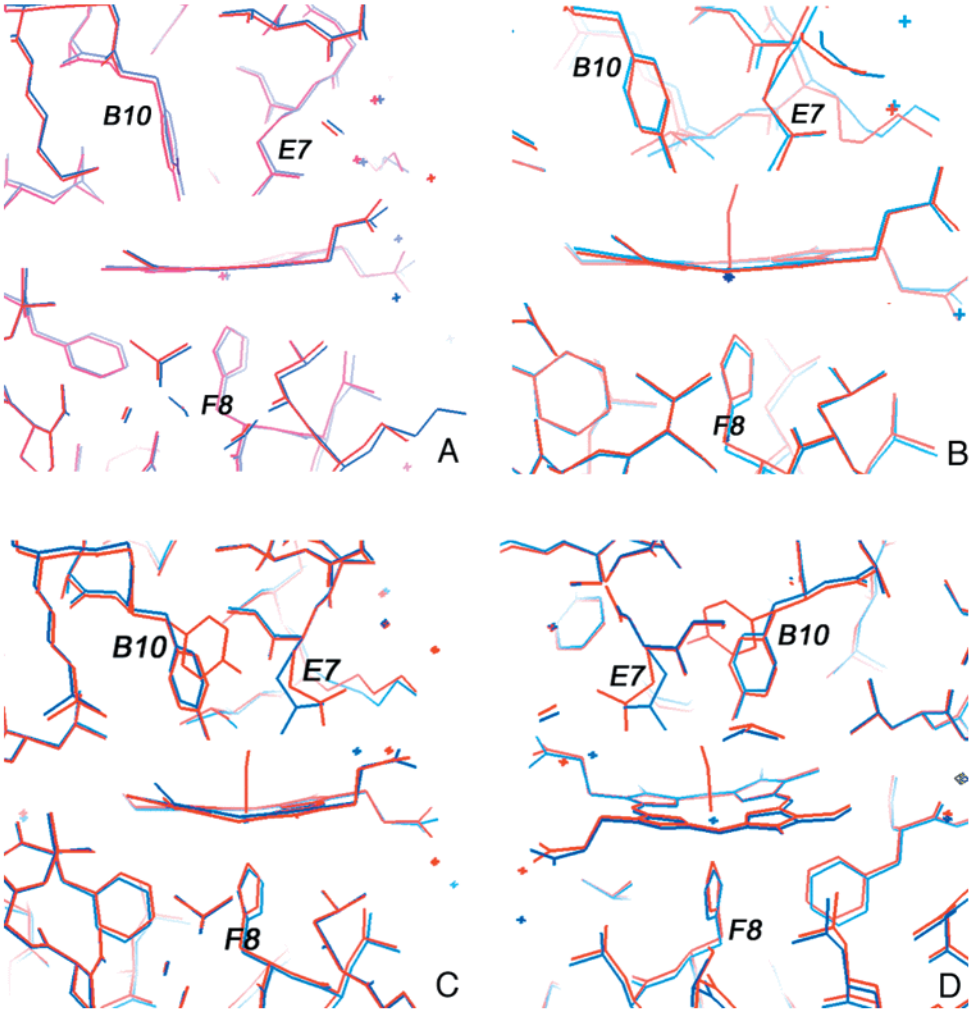

FIGURE 2: Superposition of $^{T}Hb^{YQ}$-CO (red) on $^{T}Hb^{YQ}$ (cyan) deoxy based on the BGH frame. (A) Particular of the heme pocket of α chains. (B) Side chains of amino acids lining the heme pocket of the β_2 chain. (C) Particular of heme pocket of chain β_1. The double conformation of Tyr (B10) is shown together with CO bound to the heme iron. (D) Same as panel C, but rotated by 180°.

ration, and also helix F is more displaced toward an "R-like" configuration, consistent with observations by Paoli andco-workers (*36*) on O_2 bound T-state HbA in crystal obtained from polyethylene glycol.

An unexpected feature is apparent in this doubly liganded $^{T}Hb^{YQ}$-CO on examination of the deoxy α^{YQ} chains (Figure 2A). Here, though in the distal heme pocket there is no electron density for any ligand in both $2F_o - F_c$ and $F_o - F_c$ and the water bridging Gln(E7) to the propionate is still in position, His(F8) moves very slightly toward the heme iron, shrinking the distance from 2.3 to 2.19 Å. This shift (if significant) may hint to a very initial approach to the allosteric transition.

Superposing the helices B, G, and H of one $\alpha\beta$ dimer of $^{T}Hb^{YQ}$, $^{T}Hb^{YQ}$-CO, and ^{T}HbA-O_2 on ^{T}HbA, the $\alpha_1\beta_2$ interface can be examined. In agreement with Paoli and co-workers (*36*) for ^{T}HbA-O_2 grown in low salt conditions, helices C and the corners FG of the $\alpha_1\beta_2$ interface move toward a more "R-like" conformation triggered by the displacement of the helix F, which is coupled with ligand binding to the heme iron. Communication between different subunits is also clear, judging from the shrunk distance between heme groups, and again starts from the binding of CO to the heme iron (data not shown).

Functional Properties. (i) Combination of NO. The combination of NO with HbA is insensitive to the allosteric conformation of the tetramer (or to the presence of dimers), cooperativity being expressed exclusively in the dissociation rate constants (*13*, *43*); thus, the protein reacts with this ligand at the same rate when fully unliganded (in a stopped flow experiment) or partially unliganded [in a partial photolysis experiment (*11*)] When mixed with NO, HbA combines following a single second-order process with $k = 3 \times 10^7$ M^{-1} s^{-1}; in the case of Hb^{YQ}, on the other hand, two well-separated second-order processes of equal amplitude ($k_1 = 2.3 \times 10^6$ M^{-1} s^{-1} and $k_2 = 0.4 \times 10^6$ M^{-1} s^{-1}) were observed (*22*) (Table 3). On the basis of the structural hypothesis presented above, the faster rate constant is assigned to the β^{YQ} chains in the T-state tetramer. The hybrid hemoglobin $Hb\beta^{YQ}$ reacts with NO in a single second-order process with the same rate as HbA. Interpretation of this result is difficult, but it may be attempted assuming that the wt α chains react first and that the β^{YQ} chains in the hybrid tetramer display a reactivity over-and-above that seen for the same chains in Hb^{YQ} (see above) because the allosteric transition comes into play, relieving some of the hindrance due to the mutations. In fact, the structure of the β_1 chain in the doubly liganded $^{T}Hb^{YQ}$-CO (Figure 2C) shows Tyr (B10)

Table 3: Rate Constants for Different Ligands in Their Reaction with HbA and YQ Mutants

ligand	initial state	type of experiment	HbA	Hbα^{YQ}	Hbβ^{YQ}	Hb^{YQ}
NO	^{T}Hb	"on", SF μM^{-1} s^{-1}	30(α/β)	6.0(β) 0.5(α^{YQ})	30(α)	2.3(β^{YQ}) 0.4(α^{YQ})
NO	^{R}HbO$_2$	"on", SF μM^{-1} s^{-1}	55(α/β)	22(β) (α^{YQ})	60(α) (β^{YQ})	6.0(α^{YQ}/β^{YQ})
CO	^{T}Hb	"on", SF mM^{-1} s^{-1}	130(α/β)	66(β) 7.5(α^{YQ})	63(α) 32(β^{YQ})	3.0(β^{YQ})
CO	^{R}HbCO	"on", Flash μM^{-1} s^{-1}	5(α/β)	4.5(β) (α^{YQ})	3.7(α) (β^{YQ})	1.0(α^{YQ}/β^{YQ})
O_2	^{R}HbO$_2$	"on", Flash μM^{-1} s^{-1}	47.0(α/β)	27.0	13.0 22.0	15.0 1.2
O_2	^{R}HbO$_2$	"off", replacement with CO, s^{-1}	5.3(α/β)	1.05	4.3(α) and β^{YQ}	3.9(β^{Q}) 0.5(α^{YQ})
O_2	^{R}HbO$_2$	"off", dithionite s^{-1}	21(α/β)	17 1.9	22 1.9	18(β^{YQ}) 2.5(α^{YQ})
O_2	^{T}HbO$_2$	"off", O_2 pulse s^{-1}	300(α/β)	270(β)	280(α)	130(β^{YQ})

partially out of position, suggesting an open-gate configuration. The complementary hybrid Hbα^{YQ} combines with NO in two second-order processes of equal amplitude, with rate constants of $k_1 = 6 \times 10^6$ M^{-1} s^{-1} and $k_2 = 0.5 \times 10^6$ M^{-1} s^{-1}, suggesting that the mutated α^{YQ} chains are characterized by the slower rate of combination, which is insensitive to quaternary state. However, the faster rate is not easily reconciled with the X-ray crystallographic data, which reveal that wt β chains in the unliganded ^{T}HbA and in the hybrid Hbα^{YQ} are very similar. Thus, in this hybrid, the faster NO combination rate constant is slower than expected for a wt β chain by a factor of 4, and we have no explanation for this discrepancy vis-à-vis the expectation from the simplest model.

An interesting comparison is provided by the oxidation of HbO$_2$ by NO according to reaction 2 (see the Introduction and Table 3). This process occurs on a fully oxygenated R-state hemoglobin molecule and is well described as a single second-order process in both HbA ($k = 5.5 \times 10^7$ M^{-1} s^{-1}) and Hb^{YQ} ($k = 6 \times 10^6$ M^{-1} s^{-1}). The 10-fold reduction of this rate constant, as commented before, is a significant property of Hb^{YQ} with reference to the NO scavenging effect of a possible blood substitute (*5*). In the same reaction, the hybrid Hbβ^{YQ} behaves like HbA ($k = 6 \times 10^7$ M^{-1} s^{-1}), while the other hybrid Hbα^{YQ} is oxidized a little more slowly ($k = 2.2 \times 10^7$ M^{-1} s^{-1}). In both cases, it is likely that the overall reaction is dominated by the wt partner chain. Nonetheless, it demands an enhanced reactivity of the mutated chain in the R-state hybrid hemoglobins. Since the 3D structure of the R-state of these mutants is not available, we cannot propose a structural interpretation of these data.

These experiments suggest that in both allosteric states, the mutations decrease the speed of the reaction of NO with the heme iron, consistent with the increased crowding of the heme pocket. This is seen in the oxidation induced by NO, in which the two chains of ^{R}Hb^{YQ}O$_2$ are slower than HbA by a factor of ~10, but also in the NO combination to unliganded ^{T}Hb, where the binding rate to α^{YQ} in ^{T}Hb^{YQ} deoxy is ~60-fold slower than that of the corresponding wt α chains. NO combination is rate limited by the diffusion of the ligand into the protein matrix (the so-called "external barrier"); once inside the pocket, the ligand combines easily, pointing to low activation energy for bond formation (the "internal barrier") (*11*, *12*). Therefore, the two experiments reported above probe the diffusion of NO in T and R state Hb and show, unexpectedly, that the allosteric conformation has some role in controlling the diffusion of this small diatomic molecule.

(ii) Combination of CO. In HbA, the combination of CO is strongly affected by the allosteric conformation, being ~40-fold faster in ^{R}HbA than in ^{T}HbA. The reactivity of T-state Hb, which in HbA is autocatalytic, is assessed by rapid mixing experiments, while the reactivity of the R state is probed by partial photolysis of saturated HbCO, and corresponds quite closely to that of the isolated chains (*2*). Because of its high affinity, CO readily saturates even these low-affinity mutants, which makes the interpretation of the kinetics somewhat easier than with O_2 (see below). As outlined before (*22*), the combination of CO to ^{T}Hb^{YQ} is very slow compared to ^{T}HbA (see Table 3); this is interpreted on the basis of the "hindered" structure of the distal site bearing Tyr(B10) and Gln(E7) on both chains and is consistent with similar data obtained on the analogous mutant of sperm whale Mb [called Mb-YQR (*21*)] but more extreme. The combination of CO with Hbα^{YQ} occurs in two well-separated processes, the first due to the reaction of the wt β chains and the second to the mutated α^{YQ} chains. The 2-fold smaller value for the initial rate constant (assigned to wt β chains) as compared to HbA is due to a statistical factor of 2, given the very different intrinsic reactivity of the two chains in the hybrid; the slower of the two rate constants is not too inconsistent with the binding of CO to the mutated α^{YQ} chains considering that the switch-over point is around 3 and transition to the R-state may come into play. In the case of Hbβ^{YQ}, the heterogeneity is present but not so extreme; combination with CO begins with the wt α chains (again with a consistent statistical factor of 2), and continues onto the β^{YQ} chains in a tetramer making a transition to the R-state, in which CO reactivity is enhanced (see discussion above and Figure 2, panels C and D).

The partial photolysis experiments with CO (Table 3) probing R-state reactivity contain some information of interest. In particular, it is clear that in Hb^{YQ}, R-state reactivity of the mutated chains is much faster than in the T-state, suggesting that the proximal strain adds to the effect of the barrier to diffusion, lowered by quaternary state transition.

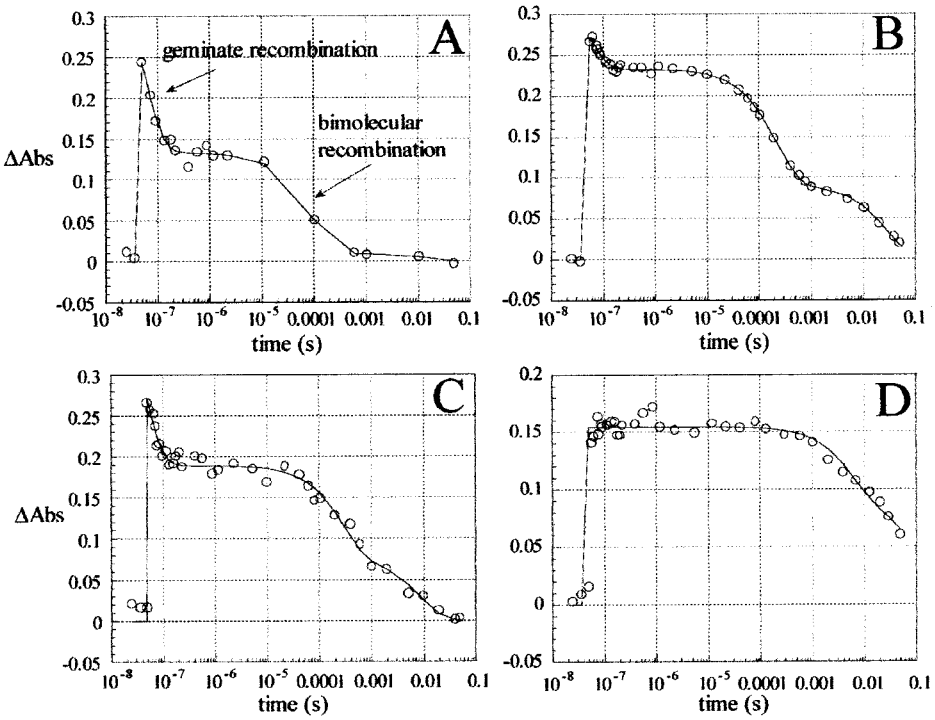

FIGURE 3: Geminate and bimolecular rebinding of CO to HbA and YQ mutant Hbs. Geminate recombination occurs within 1 μs or less after photolysis and is attributed to the rebinding of the photodissociated ligand still trapped in the distal pocket (see the arrow in panel A); bimolecular rebinding is attributed to the ligand diffusing inside the protein from the bulk (also indicated by an arrow in panel A). Experimental conditions: 0.1 M Bis-tris/HCl buffer, pH 7.0; $T = 25$ °C; CO = 1 atm; observation wavelength 436 nm. Photolysis pulse from a Nd:YAG laser, $\lambda = 532$ nm, $E = 100$ mJ, duration 5 ns. (A) HbA; (B) Hbα^{YQ}; (C) Hbβ^{YQ}; (D) Hb^{YQ}.

Differently from NO and O_2, the binding of CO is largely rate limited by the "internal barrier". The role of the "external barrier" is minimized since combination drains from an equilibrium population (small as it may be) of a complex having CO in the heme pocket. Any change in the "external barrier" affects the speed at which the equilibrium complex is populated but has a relatively small effect on the equilibrium itself. This view, which is in keeping with more refined, structure-based interpretations (*44*, *45*), is also readily testable in photolysis experiments since the noncovalent CO−Hb couple, called the geminate pair, is generated by a short laser pulse.

In HbA, CO displays no significant rebinding in the picosecond time scale, but rebinds to a significant extent in the nanosecond time range in the R-state but not in the T-state (*46*, *47*). The nanosecond geminate rebinding of CO, a probe of the reactivity of ^{R}Hb, was studied extensively in the YQ mutants. The results (Figure 3) show that (i) there is no CO geminate rebinding in R-state Hb^{YQ}, in agreement with observations on the Mb mutant carrying the same mutations (*21*), and (ii) the two hybrid Hbs have lower geminate yields than HbA (17% for Hbα^{YQ} and 30% for Hbβ^{YQ}, as compared to 47% for HBA). On the assumption that photolysis is statistical, the data indicate that the YQ mutation abolishes the geminate rebinding of CO and the geminate rebinding observed in the two hybrid Hbs has to be quantitatively assigned to the wt chain. This result demonstrates that the diffusive barrier created by overcrowding the pocket causes a reduction of the intrinsic reactivity of the heme iron, i.e. it increases the "internal barrier".

(iii) Combination and Dissociation of O_2. Oxygen resembles NO in two important aspects: its bent stereochemistry and its fast combination rate, poorly sensitive to the allosteric conformation of the molecule. The scarce kinetic cooperativity observed in the combination of O_2 to HbA implies that the equilibrium cooperativity is mainly reflected in the dissociation rate constant (*2*, *44*). Some rate constants for O_2 reactions of the mutant Hbs are reported in Table 3.

The combination of O_2 with unliganded ^{T}Hb^{YQ} followed in the stopped flow apparatus is slow and complex, extending over several decades in time; at least two significant bimolecular kinetic processes were observed with rate constants $k_1 = 1.2 \times 10^4$ M^{-1} s^{-1} and $k_2 = 2 \times 10^3$ M^{-1} s^{-1}. Both values are extremely low if compared with HbA ($^{T}k = 4 \times 10^7$ M^{-1} s^{-1}). It is important to remark that, because of the low affinity of the mutants, in the stopped flow a saturating O_2 partial pressure can barely be achieved; thus, the mutant Hb remains mostly or completely T state and reacts only partially with O_2, perhaps with an important intramolecular heterogeneity. Moreover, at some point of the reaction, the allosteric transition may occur, depending on the O_2 partial pressure, further complicating the picture. In conclusion, these experiments do not yield any interpretable information.

The overall dissociation of O_2 followed by mixing with dithionite yields an autocatalytic time course in HbA, since the T-state (characterized by a faster dissociation rate constant) is progressively populated while the overall dissociation by dithionite drives the molecule toward complete deoxygenation (*48*, *49*). Because of this, the effect of the YQ mutations on the O_2 dissociation rate constants is easier to understand following the kinetics of replacement of O_2 by CO, according to

$$Hb(O_2)_4 + 4CO \rightarrow Hb(CO)_4 + 4O_2 \qquad (4)$$

Given some straightforward assumptions, this reaction yields the O_2 dissociation rates of the R-state Hb (*2*).

As seen from the data in Table 3, in HbA a single process is observed (with $k = 5.3\ s^{-1}$); however, for Hb^{YQ}, the replacement yields two exponential processes with different rate constants (i.e. $k_1 = 3.9$ and $k_2 = 0.5\ s^{-1}$). By reference to previous work on the analogous Mb mutant [Mb-YQR (*22*)], we may expect that the additional H-bonding potential introduced by Tyr(B10) and Gln(E7) [compared to the wt residue His(E7)] may slow down the O_2 dissociation rate of Hb^{YQ}. The slower of the two rate constants reported in Table 3 probably reflects the value of the O_2 dissociation from the mutated α^{YQ} chains in the R-state tetramer; on the other hand, the faster value is assigned to the (nearly normal) dissociation from the β^{YQ} chains. Here, we imply that mutations on the distal side have a considerable (10-fold) effect on α^{YQ} chains, but no effect on β^{YQ}. This result makes good sense based on previous data by Matthews et al. (*7*) on a different mutant of HbA. These authors observed that introducing the mutation His(E7) → Gly, the O_2 dissociation rate constant of the α chains increases (~80-fold) because the H-bond between bound O_2 and His (E7) is lost. However, this effect was not seen when the same mutation was introduced into the β chains, in agreement with the absence of the H-bond between His (E7) and O_2 in those chains (*50*). The replacement data on mutant $Hb\beta^{YQ}$ (Table 3) are fully consistent with this simple interpretation.

As outlined above, the overall dissociation by dithionite is more complex. As shown in Table 3, the double mutant Hb^{YQ} dissociates O_2 in two exponential processes, indicative of intramolecular heterogeneity. We assign the faster rate (practically identical to R-state k_{off} of HbA) to the β^{YQ} chains, while the slower one is due to the α^{YQ} chains, whose O_2 dissociation rate seems independent of quaternary state, but dependent on distal H-bonding potential. Not surprisingly, intramolecular heterogeneity shows up also in the case of the hybrid Hbs.

The dissociation of O_2 from the T-state was studied by Gibson's pulse method (*51*). In this experiment, only a low fractional saturation with O_2 is achieved in the first mixing, and thus, the dissociation rate constant measured after mixing with excess dithionite pertains to the oxygenated sites only. The two hybrid tetramers dissociated O_2 at exactly the same rate constant as HbA, which is consistent with the fact that the mutated chains combine much too slowly with O_2 and thus they would be poorly oxygenated or not at all; thus, the wt chains dominate the reaction. In the case of Hb^{YQ}, the observed rate constant ($130\ s^{-1}$) is slower than that of the other proteins ($270-300\ s^{-1}$, see Table 3), but much faster than those determined for the R-state mutant Hb^{YQ} (3.9 and $0.5\ s^{-1}$). On the basis of the structure, we believe that in the O_2-pulse experiment starting with Hb^{YQ}, the measured "off" rate constant ($^Tk = 130\ s^{-1}$) pertains only to the mutated β^{YQ} chains, which combine more rapidly with ligands and display a large effect of the allosteric state on the rate of O_2 dissociation (but a small or insignificant effect of the distal site structure). This result is qualitatively consistent with the observation that Hb^{YQ} (though low affinity) binds O_2 in a cooperative fashion (*22*).

DISCUSSION

We have characterized by kinetics and crystallography three mutants of human HbA (called YQ) bearing the two distal-site mutations Leu (B10) → Tyr and His (E7) → Gln. The tetramers with the two mutations either on the α chains ($Hb\alpha^{YQ}$) on the β chains ($Hb\beta^{YQ}$), or both (Hb^{YQ}) display clear-cut and reproducible modifications in the reactivity toward the gaseous ligands O_2, CO, and NO. Despite considerable complexities, the kinetic data seem (by-and-large) consistent with a simple set of rules which emerge from examination of the crystallographic structures of the deoxygenated mutants and of a partially CO-bound Hb^{YQ} in the T-state, as compared to HbA.

The structural data show unequivocally that all the mutants in the deoxygenated state have a quaternary structure corresponding to the T allosteric state with intact and "canonical" interfaces (*31*). Upon complete saturation with O_2 or CO, these mutants undergo a T-to-R allosteric transition, as indicated not only by cooperativity ($n = 1.7-2.3$ for the various mutants) but also by visible and near-UV optical spectroscopy (*22*). Thus, to understand the effects of the two mutations on heme reactivity, we attempted an interpretation of the kinetic data taking into account not only the effects of the R-to-T allosteric transition, based on the extensive knowledge available on HbA (*41*), but also the results obtained on a similar mutant of sperm whale myoglobin, called Mb-YQR (*21*). In this mutant, it was shown that (i) the combination rate constant for O_2 is decreased (by ~10-fold) because the two new side chains move toward the heme iron upon deoxygenation, and (ii) the dissociation rate constant is also reduced by ~10-fold, due to the increased H-bonding potential provided by Tyr and Gln in the distal heme pocket. The comments reported in the Results detail the level of validity of the MWC two state model (*32*) for an interpretation of all the kinetic constants (Table 3), taking into account the modifications in intrinsic heme reactivity of the two chains due to the mutations.

The crystallographic structure of the mutants in the T-state (see Figure 1 and Table 2), which shows that the heme pocket of β^{YQ} chains should be more accessible to a ligand compared to the α^{YQ}, provides a clear rationalization of the heterogeneity observed in some of the kinetic experiments. Thus, in addition to the finding that the overall combination rate constants are reduced by 10−50-fold compared to ^{T}HbA [consistent with observations on Mb-YQR (*21*)], we tentatively assigned the slowest combination phase to the α^{YQ} chains. This result is clearly exemplified by the reactions with NO starting either from the deoxy T-state or from the oxygenated R-state (see Table 3). In support of this hypothesis, the crystallographic data on the doubly liganded Hb^{YQ}-CO in the T-state (see Figure 2, panels C and D) show that CO is bound only to the β^{YQ} chains, strengthening the assignment of the kinetic constants. The intrinsic heterogeneity of the two chains in $^THb^{YQ}$ allows also to interpret the kinetic results obtained on the two hybrid tetramers, as detailed above.

The kinetic properties of the R-state mutants are best discussed by analyzing the dissociation rate constants for O_2. We know that in the mutant Mb-YQR (*21*) the O_2 "off" rate is reduced compared to the wt protein because of the

increased H-bonding potential provided by Tyr(B10) and Gln(E7), compared to His (E7) present in wt Mb. Moreover, it was shown that, in the case of HbA, the stabilizing effect exerted by the O_2−His (E7) H-bond is large for the α chains but absent in the β chains (*7*); this result is consistent with the crystallographic structure of oxygenated HbA (*50*). Consistently, we find that the effect of the mutated side chains on the O_2 "off" rate is large (∼10-fold) for the α^{YQ} chains in $^{R}Hb^{YQ}$, but essentially absent in the β^{YQ} chains (see data in Table 3 on the replacement of O_2 by CO). This interpretation also affords a satisfactory first-order understanding of the behavior of the two hybrids (see Results).

Moreover, we have direct evidence for an effect of the R-to-T transition on the kinetic constants of the mutant Hbs from several of the experiments reported above. A particularly clear-cut case is endowed by the O_2 dissociation rate constant of the β^{YQ} chains which increases from 3.9 s^{-1} in the R-state to 130 s^{-1} in the T-state (as shown by the so-called O_2 pulse experiment). On the other hand, analysis of the kinetic data suggests that the allosteric transition has essentially no effect on the O_2 dissociation rate of the α^{YQ} chains since here the barrier is dominated by the enhanced H-bonding potential imposed by the mutated distal side residues.

An effect of the T quaternary state on the reactivity of the β^{YQ} chains is also supported by the crystallography of the doubly liganded $^{T}Hb^{YQ}$-CO. As shown in Figure 2, panels C and D, the ligand bound to one of the β chains (called β_1^{YQ}) is associated to a motion of Tyr(B10), which appears to swing (partially) out of the pocket, mimicking the opening of a "gate". On the other hand, the structure of the other β chain (called β_2^{YQ}) is different because of crystal packing constraints. We believe that the structure of the two CO-bound β^{YQ} chains in this doubly liganded $^{T}Hb^{YQ}$-CO may picture two distal site "snapshots" of different events occurring upon ligation of T-state Hb^{YQ}, thus providing a novel piece of structural information on the mechanism of T-state ligation and on the control of heme reactivity by local distal-site residues. Our ligation intermediates, like those obtained by Paoli et al. (*36*) and by Miyazaki et al. (*40*), have intact C-terminal salt bridges donated by the β chains, and do not reveal motion of Tyr (HC2) from their pockets (*42*). Breaking of these salt bridges is associated to proton release, occurs in solution upon ligation of T-state Hb, and accounts for the tertiary Bohr effect of ^{T}HbA, characteristically absent in ^{T}Hb crystals (*52*). In Hb^{YQ}, the order of ligand binding is reversed with respect to HbA, and the α chains combine with ligands after the β chains (*39*, *42*). Given that the structural contribution of the two types of subunits to the allosteric transition is not the same (*53*, *54*), being expressed mostly on the "proximal" side of the heme for the α chains and predominantly on the "distal" side in the β chains (*42*), it is possible that the reversed order of ligation observed in Hb^{YQ} is linked to its lower cooperativity.

The biotechnological task of producing a satisfactory Hb-based blood substitute, still to be achieved, has progressed considerably due to site-directed mutagenesis (*55*). Some of the side effects of Hb preparations for intravenous administration (i.e., renal toxicity, short half-life and high oxygen affinity) have already been overcome, and it seems that the hypertensive effect of free Hb, linked to scavenging of NO, may be minimized (*5*). This paper demonstrates that it is possible to synthesize by site-directed mutagenesis Hb variants with low O_2 affinity, low rate of autoxidation and reduced NO reactivity. The latter effect is achieved by mutating amino acid residues which control the ligand diffusion inside the protein moiety, given that the activation energy for formation of the Fe−NO bond is so low. Although the effects of the YQ mutations may not completely fulfill all the requirements of a Hb-based blood substitute, nonetheless they suggest a rational strategy for controlling the reactivity toward such a difficult ligand as NO.

ACKNOWLEDGMENT

We gratefully acknowledge Somatogen Inc. (CA) for permission to use their Hb expression system in *E. coli*. Dr. Nicolini and Mr. Dagai of ISS (Rome) are gratefully acknowledged for large scale fermentation of *E. coli*. The authors would like to thank Dr. Max Paoli (Cambridge, UK) for the permission to use the nondeposited coordinates of $^{T}HbA\text{-}O_2$ for comparison. Special thanks to Dr. Stefania Contardi for typing and editing the manuscript.

REFERENCES

1. Riggs, A. F. (1991) *Curr. Opin. Struct. Biol. 1*, 915−921.
2. Antonini, E., and Brunori, M. (1971) *Hemoglobin and Myoglobin in their reactions with ligands*, North-Holland Publishing Co., Amsterdam.
3. Winslow, R. M. (1995) *Nat. Med. 1*, 1212−1215.
4. Alayash, A. I. (1999) *Nat. Biotechnol. 17*, 545−549.
5. Doherty, D. H., Doyle M. P. Curry, S. R., Vali, R. J., Fattor, T. J., Olson, J. S., and Lemon, D. D. (1998) *Nat. Biotechnol. 16*, 672−676.
6. Perutz, M. F. (1979) *Annu. Rev. Biochem. 48*, 327−386.
7. Matthews, A. J., Rholfs, R. J., Olson, J. S., Tame, J. R., Renaud, J. P., and Nagai, K. (1989) *J. Biol. Chem. 20*, 16573−16583.
8. Springer, B. A., Sligar, S. G., Olson, J. S., and Phillips, G. N., Jr. (1994) *Chem. Rev. 94*, 699−714.
9. Perutz, M. F. (1989) *Trends Biochem. Sci. 2*, 42−44.
10. Olson, J. S., Mathews, A. J, Rohlfs, R. J., Springer, B. A., Egeberg, K. D., Sligar, S. G., Tame, J. R., Renaud, J. P., and Nagai, K. (1998) *Nature 336*, 265−266.
11. Morris, R. J., and Gibson, Q. H. (1980) *J. Biol. Chem. 255*, 8050−8053.
12. Olson, J. S., and Phillips, G. N. (1996) *J. Biol. Chem. 271*, 17593−17596.
13. Moore, E. G., and Gibson, Q. H. (1976) *J. Biol. Chem. 251*, 2788−2794.
14. Gibson, Q. H., Ikeda-Saito, M., and Yonetani, T. (1985) *J. Biol. Chem. 260*, 14126−1431.
15. Scott, E. E., Gibson, Q. H., and Olson, J. S. (2001) *J. Biol. Chem. 276*, 5177−5188.
16. De Baere, I., Perutz, M. F., Kiger, L., Marden, M. C., and Poyart, C. (1994) *Proc. Natl. Acad. Sci. U.S.A. 91*, 1594−1597.
17. Bartnicki, D. E., Mizukami, H., and Romero-Herrera, A. E. (1983) *J. Biol. Chem. 258*, 1599−1602.
18. Waterman, M. R., Stenzel, P. (1974) *Biochim. Biophys. Acta 359*, 401−410.
19. Brantley, R. E., Jr., Smerdon, S. J., Wilkinson, A. J., Singleton, E. W., and Olson, J. S. (1993) *J. Biol. Chem. 268*, 6995−7010.
20. Travaglini-Allocatelli, C., Cutruzzolà, F., Brancaccio, A., Vallone, B., and Brunori, M. (1994) *FEBS Lett. 352*, 63−66.
21. Brunori, M., Cutruzzolà, F., Savino, C., Travaglini-Allocatelli, C., Vallone, B., and Gibson, Q. H. (1999) *Biophys. J. 76*, 1259−1269.

22. Miele, A. E., Santanché, S., Travaglini-Allocatelli, C., Vallone, B., Brunori, M., and Bellelli, A. (1999) *J. Mol. Biol. 290*, 515−524.
23. Looker, D., Abbott-Brown, D., Cozart, P., Durfee, S., Hoffman, S., Mathews, A. J., Miller-Roehrich, J., Shoemaker, S., Trimble, S., Fermi, G., Komiyama, N. H., Nagai, K., and Stetler, G. (1992) *Nature 356*, 258−260.
24. Perutz, M. F. (1968) *J. Cryst. Growth 2*, 54−56.
25. Otwinowsky, Z., and Minor, W. (1996) *Methods Enzymol. 276*, 307−325.
26. Murshdov, G., Vagin, A., and Dodson, E. (1997) *Acta Crystallogr., Sect. D 53*, 240−255.
27. Collaborative Computational Project Number 4 (1994) *Acta Crystallogr., Sect. D 50*, 760−763.
28. Fermi, G, Perutz, M., Shanaan, B., and Fourme, R. (1984) *J. Mol. Biol. 175*, 159−174.
29. Laskowski, R. A., MacArthur, M. W., Moss, D. S., and Thorntorn, J. (1993) *J. Appl. Crystallogr. 26*, 283−291.
30. Imai, K., and Yonetani, T. (1973) *Biochem. Biophys. Res. Commun. 50*, 1055−1060.
31. Perutz, M. F., Fermi, G., Luisi, B., Shaanan, B., and Liddington, R. C. (1987) *Acc. Chem. Res. 20*, 309−321.
32. Monod, J. Wyman, J., and Changeux, J. P. (1965) *J. Mol. Biol. 12*, 88−118.
33. Henry, E. R., Jones, C. M., Hofrichter, J., and Eaton, W. A. (1997) *Biochemistry 36*, 6511−6528.
34. Tame, J., and Vallone, B. (2000) *Acta Crystallogr., Sect. D 56*, 805−811.
35. Perutz, M. F. (1970) *Nature 228*, 726−739.
36. Paoli, M., Liddington, R., Tame, J., Wilkinson, A., and Dodson, G. (1996) *J. Mol. Biol. 256*, 775−792.
37. Liddington, R., Derewenda, Z., Dodson, E., Hubbard, R., and Dodson, G. (1992) *J. Mol. Biol. 228*, 551−579.
38. Bettati, S., Mozzarelli, A., Rossi, G. L., Tsuneshige, A., Yonetani, T., Eaton, W. A., and Henry, E. R. (1996) *Proteins 25*, 425−437.
39. Mozzarelli, A., Rivetti, C., Rossi, G. L., Eaton, W. A., and Henry, E. R. (1997) *Protein Sci. 6*, 484−489.
40. Miyazaki, G., Morimoto, H., Yun, K. M., Park, S. Y., Nakagawa, A., Minagawa, H., and Shibayama, N. (1999) *J. Mol. Biol. 292*, 1121−1136.
41. Eaton, W. A., Henry, E. R, Hofrichter, J., and Mozzarelli, A. (1999) *Nat. Struct. Biol. 6*, 351−358.
42. Perutz, M. F., Wilkinson, A. J., Paoli, M., and Dodson, G. G. (1998) *Annu. Rev. Biophys. Biomol. Struct. 27*, 1−34.
43. Cassoly, R., and Gibson, Q. H. (1975) *J. Mol. Biol. 91*, 301−313.
44. Szabo, A. (1978) *Proc. Natl. Acad. Sci. U.S.A. 75*, 2108−2111.
45. Moffat, K., Deatherage, J. F., and Seybert, D. W. (1979) *Science 206*, 1035−1042.
46. Hofrichter, J., Henry, E. R., Sommer, J. H., Deutsch, R., Ikeda-Saito, M., Yonetani, T., and Eaton, W. A. (1985) *Biochemistry 24*, 2667−2679.
47. Jongeward, K. A., Magde, D., Taube, D. J., Marsters, J. C., Traylor, T. G., and Sharma, V. S. (1988) *J. Am. Chem. Soc. 110*, 380−387.
48. Hopfield, J. J., Shulman, R. G., and Ogawa, S. (1971) *J. Mol. Biol. 61*, 425−443.
49. Schulman, R. G., Hopfield, J. J., and Ogawa, S. (1975) *Q. Rev. Biophys. 8*, 325−420.
50. Shaanan, B. (1983) *J. Mol. Biol. 171*, 31−59.
51. Gibson, Q. H. (1973) *Proc. Natl. Acad. Sci. U.S.A. 70*, 1−4.
52. Bettati, S., Mozzarelli, A., and Perutz, M. F. (1998) *J. Mol. Biol. 281*, 581−585.
53. Perutz, M. F., Wilkinson, A. J., Paoli, M., and Dodson, G. G. (1998) *Annu. Rev. Biophys. Biomol. Struct. 27*, 1−34.
54. Barrick, D., Ho, N. T., Simplaceanu, V., Dahlquist, F. W., and Ho, C. (1997) *Nat. Struct. Biol. 4*, 78−83.
55. Olson, J. S., Eich, R. F., Smith, L. P., Warren, J. J., and Knowles, B. C. (1997) *Artif. Cells Blood Substitutes, Immobilization Biotechnol. 25*, 227−241.

BI011602D